Annals of Biomedical Engineering, Vol. 33, No. 5, May 2005 (© 2005) pp. 603–615
DOI: 10.1007/s10439-005-2397-3

Polarization of a Spherical Cell in a Nonuniform Extracellular Electric Field

DONGCHUL C. LEE[1] and WARREN M. GRILL[1,2]

[1]Department of Biomedical Engineering, Case Western Reserve University;
[2]Department of Biomedical Engineering, Duke University

(Received 2 February 2004; accepted 20 December 2004)

Abstract—Polarization of cells by extracellular fields is relevant to neural stimulation, cardiac pacing, cardiac defibrillation, and electroporation. The electric field generated by an extracellular electrode may be nonuniform, and highly nonuniform fields are produced by microelectrodes and near the edges of larger electrodes. We solved analytically for the transmembrane voltage (Φ_m) generated in a spherical cell by a nonuniform extracellular field, as would arise from a point electrode. Φ_m reached its steady state value with a time constant much shorter than the membrane time constant in both uniform and nonuniform fields. The magnitude of Φ_m generated in the hemisphere of the cell toward the electrode was larger than in the other hemisphere in the nonuniform field, while symmetric polarization occurred in the uniform field. The transmembrane potential in oocytes stained with the voltage sensitive dye Di-8-ANEPPS was measured in a nonuniform field at three different electrode-to-cell distances. Asymmetric biphasic polarization and distance-dependent patterns of membrane voltage were observed in the measurements, as predicted from the analytical solution. These results highlight the differences in cell polarization in uniform and nonuniform electric fields, and these differences may impact excitation and poration by extracellular fields.

Keywords—Electrical stimulation, Laplace's equation, Nerve modeling, Voltage sensitive dye.

INTRODUCTION

The polarization of cells can modulate the outputs of cardiac and neural tissues, and is relevant to neural stimulation, cardiac pacing and defibrillation, and electroporation. The spatial and temporal pattern of transmembrane voltage generated by an extracellular electric field is determined by the shape of the cell, its membrane properties, and the characteristics and orientation of the extracellular electric field with respect to the cell.[11] The transmembrane voltage (Φ_m) generated in spheroidal,[2,5,17,20,21,27] ellipsoidal[3,12] and cylindrical cells[23,25,36] has been determined for spatially uniform extracellular electric fields.

Address correspondence to Warren M. Grill, PhD., Duke University, Department of Biomedical Engineering, Box 90281, Durham, North Carolina 27708-0281. Electronic mail: warren.grill@duke.edu

However, the extracellular electric field is always nonuniform (nonhomogeneous) except between two parallel plate electrodes, and the nonuniformity is most apparent in the electric fields from small electrodes,[28] near the edges of larger electrodes, and near boundaries between tissues with different conductivities. The resulting Φ_m may differ from that generated by a uniform extracellular field. When considering stimulation in the central nervous system, e.g., brain microstimulation[9] or intraspinal microstimulation[13,18,30,31] the cell body is relatively large compared to the other neural elements (axons, dendrites). A cell body with a large volume can influence the electric field locally around the cell and violate the assumptions of classical cable theory.[35]

The purpose of this study was to determine the temporal and spatial pattern of Φ_m generated in a spherical cell by a nonuniform extracellular electric field. The Φ_m was obtained by determining analytical solutions for the electrical potentials in the intracellular and extracellular spaces generated by a nonuniform extracellular field in the presence of a spherical cell body, and solving for the Φ_m generated by that electric field. The results (electric field distribution and Φ_m) were compared to those obtained when ignoring the alteration of the potential distribution by the presence of the cell, as well as the results obtained in a uniform extracellular field. To verify the transmembrane voltage generated in a spherical cell exposed to a nonuniform electric field, optical measurements of transmembrane voltage were conducted in spherical cells using a voltage sensitive dye (Di-8-ANEPPS).[6,15,26,39]

METHODS

Expressions for the intracellular and extracellular potentials were derived by solving Laplace's equation with the proper boundary conditions. The transmembrane voltage, Φ_m, was computed as the voltage difference between the intracellular and extracellular potentials at the membrane boundary. The analytical solution was compared to the estimated Φ_m measured from fluorescence images of oocytes

TABLE 1. Definition, unit and value of symbols used in analytical solution.

Symbol	Definition	Unit	Typical value
R_m	Specific membrane resistance	KΩ cm^2	200
C_m	Specific membrane capacitance	μF cm^{-2}	1
σ_i	Intracellular conductivity	S cm^{-1}	0.014
σ_e	Extracellular conductivity	S cm^{-1}	0.002
Φ_i	Intracellular potential	mV	
Φ_e	Extracellular potential	mV	
Φ_m	Transmembrane voltage ($\Phi_m = \Phi_i - \Phi_e$)	mV	
R	Cell radius	μm	10–60
U	Distance to the electrode from an evaluation point	μm	
d	Electrode-to-cell distance	μm	
r	Radial distance from the origin to an evaluation point	μm	
t	Time	ms	
τ_c	Cell time constant	ms	
τ_m	Membrane time constant	ms	

loaded with Di-8-ANEPPS in a nonuniform electric field generated by a metal microelectrode.

Analytical Methods

A cell was modeled as a sphere, with the membrane (specific membrane resistance, $R_m = 200\,\mathrm{K\Omega\,cm^2}$; specific membrane capacitance, $C_m = 1\ \mu\mathrm{F/cm^2}$) modeled with zero thickness,[11,21] positioned in a homogeneous isotropic medium in the vicinity of a point source of current with the return (counter) electrode positioned at infinity. The intracellular (Φ_i) and extracellular potential (Φ_e) were solved from Laplace's Eqs. (1)–(3), because the divergence of the current density is zero everywhere in the internal and external media.

$$\nabla^2\Phi_i = 0 \tag{1}$$

$$\Phi_e = \Phi_{es} + \Phi_{applied} \tag{2}$$

$$\nabla^2\Phi_{es} = 0, \quad \Phi_{applied} = \frac{I}{4\pi\sigma_e U} \tag{3}$$

where Φ_{es} is the secondary potential outside the sphere,[1,33] which must satisfy Laplace's equation, I is the applied current, $\sigma_e = 0.002$ S/cm is the extracellular conductivity,[10,32] and U is the distance from the point source of current to the evaluation point. The cell membrane forms a boundary between the intracellular and extracellular domains and the requirement for continuity of the normal component of current gives rise to two boundary conditions at $r = R$, (R: the cell radius)[2,5,36]:

$$\sigma_i\frac{\partial\Phi_i}{\partial r} = C_m\frac{\partial\Phi_m}{\partial t} + \frac{\Phi_m}{R_m}, \quad \Phi_m = \Phi_i - \Phi_e \tag{4}$$

$$\sigma_i\frac{\partial\Phi_i}{\partial r} = \sigma_e\frac{\partial\Phi_e}{\partial r}, \tag{5}$$

where r is the normal to the cell surface and $\sigma_i = 0.014$ S/cm is the conductivity of the intracellular medium.[8] The initial Φ_m was set to 0 mV by defining potential = 0 mV everywhere.

An example, showing the solutions for the intracellular potential is given by Eqs. (6)–(9), and illustrates that the solutions were a summation of associated Legendre functions ($P_m^0[\cos\theta]$) with coefficients A_m computed from conditions defining the boundaries and the current source. X is the ratio ($X = d/R$) between the electrode-to-cell distance, d, measured from the center of the cell to the tip of the electrode, and the cell radius, R. Complete details and other solutions are provided in the Appendix.

$$\Phi_i = \sum_{m=0}^{\infty} A_m r^m P_m^0[\cos\theta] \tag{6}$$

$$A_m = \frac{a_2}{a_1}S_c(1 - e^{-a_1 t}) \tag{7}$$

$$\frac{a_2}{a_1} = \left[R^{-m}\left(-\int_0^{\pi}\frac{(1 - X\cos\theta)\ \sin\theta P_m[\cos\theta]}{(1 + X^2 - 2X\cos\theta)^{3/2}}d\theta + (1+m)\int_0^{\pi}\frac{\sin\theta P_m[\cos\theta]}{\sqrt{1 + X^2 - 2X\ \cos\theta}}d\theta\right)\right] \Big/ \left[4\pi\sigma_i\sigma_e R_m\left(\frac{1+m}{m}\right)\int_0^{\pi}\sin\theta\ P_m[\cos\theta]^2\,d\theta\right] \tag{8}$$

$$a_1 = \frac{1}{R}\frac{\sigma_e\sigma_i}{C_m((1+m)\sigma_e + m\sigma_i)}\frac{1+m}{m} \tag{9}$$

The Φ_m generated by a uniform extracellular field was solved by Schwan,[37] and the time-dependent solution as a function of radial position was obtained analytically by Kotnik *et al.* (1998) and is given by

$$\Delta\Phi_m = f \times E \times R\ \cos\theta\left[1 - \exp\left(-\frac{t}{\tau}\right)\right] \tag{10}$$

$$\tau = \frac{RC_m}{\frac{2\sigma_e\sigma_i}{2\sigma_o + \sigma_i} + \frac{R}{h}\sigma_m}, \tag{11}$$

where E is the strength of the electric field, R is the cell radius, h is the membrane thickness, σ_m, σ_i, and σ_e are conductivity of membrane, intracellular medium, and extracellular medium, and $f \approx 3/2$ under the condition that $\sigma_m \ll \sigma_i, \sigma_e$.[22] To compare the pattern of Φ_m generated in a nonuniform field to the Φ_m generated in a uniform field, the magnitude of cosine function was scaled to match the maximally polarized point generated by the nonuniform field.

Experimental Methods

Immature Xenopus oocytes were collected and stained with a solution of ND96 (96 mM NaCl, 2 mM KCl, 1.8 mM CaCl, 1 mM $MgCl_2$ and 5 mM HEPES; pH 7.5 adjusted with NaOH, osmolarity ≈200 mosM) with 200 μM of Di-8-ANEPPS for 30 min in room temperature.[6,40] After the staining process, oocytes were transported to a Petri dish with artificial extracellular medium consisting of de-ionized water with sucrose (21.395 g/l ≈120 mosM) added to increase the osmolarity of the solution.[34]

To create a nonuniform electric field, a tungsten microelectrode was placed at the center of the dish with a ring-shaped silver return electrode along the perimeter of the dish (see Fig. 9). The microelectrode was insulated except at the tip, and created an electric field approximating a true point source.[28] Rectangular 100 ms duration current pulses (PULSAR, FHC Inc., Bowdoinham, ME) were delivered through the microelectrode positioned at three different electrode-to-cell distances determined by visual inspection. As the distance from the electrode to the cell was increased, the stimulation intensity was increased (range = 3–20 μA) to maintain a similar magnitude of transmembrane polarization and thereby increase the signal-to-noise ratio.

Image (1392 × 1040 size) acquisition was controlled by Metafluor software (Universal Imaging, West Chester, PA), and the acquired fluorescence signals were integrated by a cooled 12-bit digital CCD camera (PXL, Photometrics, Tucson, AZ). Fluorescence was excited at 480 nm and detected at >550 nm with a Nikon microscope equipped with an externally controlled light source (Lambda DG-4, Sutter Instrument Company, Novato, CA).

Fluorescence images were acquired in the control state (C image) before applying the electric field, and during delivery of the current pulse (S image). The exposure time was 100 ms. Five pulses of 100 ms pulse width were delivered with 1 s interpulse intervals. The control images (C1–C5) were collected 500 ms before each current pulse, and the stimulated images (S1–S5) were collected during the pulse. Ensemble averages (C_{avg} and S_{avg}) of five images C1–C5 and S1–S5 were computed to increase the signal-to-noise ratio, and the fluorescence difference was computed as $\Delta F/F = (C_{avg} - S_{avg})/C_{avg}$[26] to obtain a signal proportional to the change in transmembrane potential generated by the applied field.

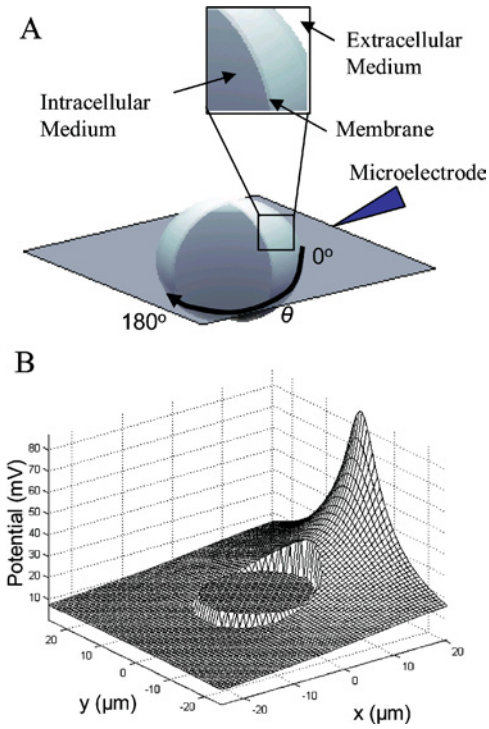

FIGURE 1. Model of a spherical cell in a nonuniform electric field. (A) The membrane separating the intracellular space and extracellular space was modeled with passive properties including a membrane resistance in parallel with a membrane capacitance. (B) Potentials in the extracellular and intracellular space, obtained from analytical solutions to Laplace's equation. The spherical cell (radius 10 μm) was centered at (0, 0), and the electrode was positioned 25 μm away as in A.

RESULTS

The electric potentials in the extracellular and intracellular spaces were obtained by solution of Laplace's equation during extracellular electrical stimulation through a point source electrode. Subsequently, the transmembrane voltage (Φ_m) was computed as the potential difference across the membrane. The Φ_m in a nonuniform field was compared to that in a uniform field and the sensitivity of the pattern of polarization in the nonuniform field to the physiological environment was studied by varying the values of model parameters. The analytical solution was compared to fluorescence imaging of the Φ_m generated in oocytes by a nonuniform electric field.

Distribution of Intracellular and Extracellular Potentials

Due to axial symmetry, the potential on a plane bisecting the center of the sphere and the current source adequately represented the potential in the whole space. The steady state potentials in the intracellular ($r < R$) and extracellular spaces ($r \geq R$) are plotted in Fig. 1. The extracellular potential was inversely related to the distance between the current

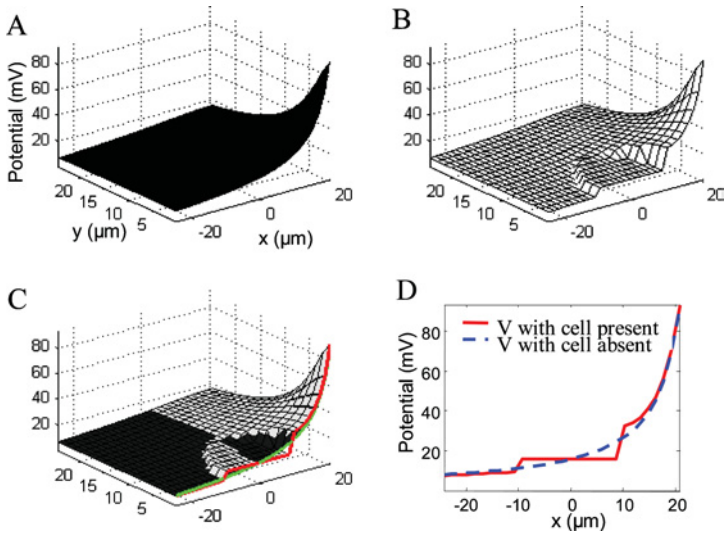

FIGURE 2. Effect of the presence of the cell on the electric potential. (A) Potential without the cell present. (B) Potentials in the extracellular and intracellular space with cell present. (C) Superimposed potentials from A and B. The presence of the cell increased the potential outside of the hemisphere toward the electrode and attenuated the potential on other side. (D). Potential profiles along a line crossing the electrode and the center of the cell. Electrode and cell positioned as in Fig. 1.

source and measurement point. The spatial gradient of the potential was much steeper in the extracellular space than in the intracellular space, and the intracellular potential was approximately uniform due to the highly conductive cytoplasmic medium. At the boundary between the intracellular and extracellular media, a potential across the membrane was produced. Details of the transmembrane voltage as a function of radial position and time are described below.

The electric field was altered by the presence of the cell. Figure 2(A) and 2(B) show the distribution of potentials calculated with and without the cell present. The electric field generated by a point source in free space was nonuniform and decayed in inverse proportion to the distance to the source. The presence of the cell increased the magnitude of the potentials outside of the membrane toward the electrode and attenuated the magnitude of the potentials on the other side. The presence of the cell affected the distribution of extracellular potentials and thus the resulting transmembrane voltages (see below).

Temporal Evolution of the Potential Distribution

At time $= 0$ before stimulation was applied, the potential everywhere was 0 V. When the stimulation was turned on ($t = 0+$), the electric potential was continuous [Fig. 3(A)] across the membrane, because the membrane capacitance was not yet charged. As time increased, the membrane capacitance charged and the potential was discontinuous between the intracellular and extracellular spaces [Fig. 3(B)]. The potentials reached steady state [Fig. 3(C)] within 2 μs with the default parameters in Table 1 (see below for sensitivity analysis).

Transmembrane Voltage in Nonuniform Extracellular Field

The Φ_m was obtained as the difference between the intracellular and extracellular potentials at $r = R$ (Fig. 4) and plotted as a function of the angle (θ) from an axis running through the electrode and the center of the cell where 0° corresponds to the point nearest to the electrode. The polarization pattern along the membrane exhibited regions of both hyperpolarization and depolarization, while current injection through an intracellular microelectrode produced monophasic polarization. The magnitude of polarization was asymmetric and characterized by highly focused polarization with large magnitude over the area near to the electrode and less pronounced polarization over the rest of the sphere. The point of zero polarization, or neutral point, defined as $\Phi_m = 0$ V was located at ~78° [Fig. 4(B)]. For the cell with radius of 10 μm, the Φ_m reached steady state within 2 μs [Fig. 4(C)].[15] The cellular time constant (τ_c)[5,15,24] was obtained from the voltage response assuming the cell behaved as a first-order linear system, and was substantially less than the membrane time constant ($\tau_m = 200$ ms) which is the product of the membrane resistance and the membrane capacitance.

The degree of asymmetry increased and location of the point of zero polarization shifted farther from the equator (90°) as the electrode-to-cell distance decreased. To compare the patterns of Φ_m at different electrode-to-cell distances, the Φ_m obtained at the longer distance was normalized by the maximum depolarization at the shorter electrode-to-cell distance [Fig. 5(A)]. While the relative amount of polarization in the hemisphere opposite the electrode was relatively unaffected by the electrode-to-cell

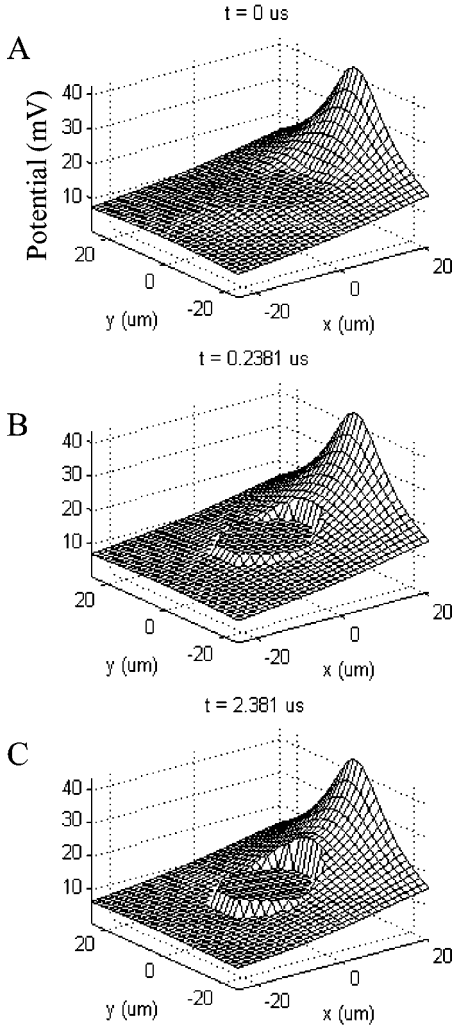

FIGURE 3. Potential as a function of time on the plane crossing the electrode and center of the cell. (A) At $t = 0+$ the stimulation was on and the potential across the membrane is continuous because the membrane capacitance was not yet charged. (B) In the middle of the charging phase, the intracellular potential approached steady state. (C) The extracellular potential reached steady state in ~2 μs.

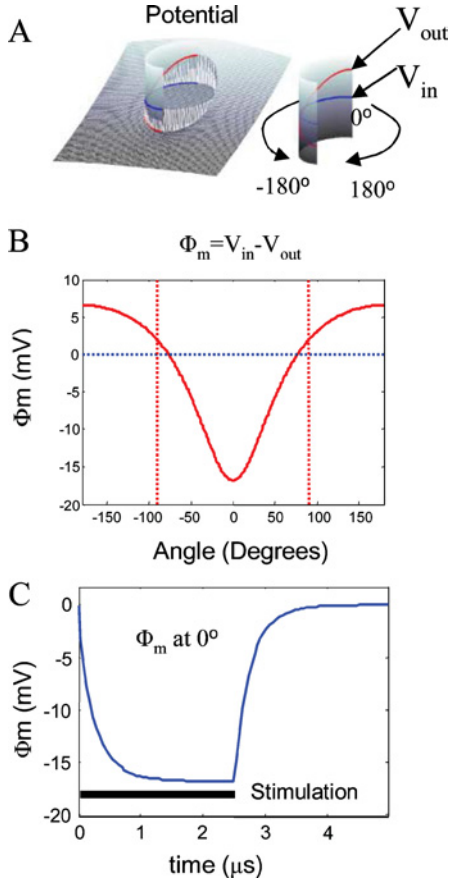

FIGURE 4. The transmembrane voltage, Φ_m, was computed from the potential difference across the membrane. (A) Solutions for intracellular and extracellular potential at $r = R$ on the plane were obtained from Eqs. (1) and (2). (B) Φ_m as a function of the angle around the cell, where 0° is the point nearest to the electrode and 180° is on the opposite side. The hemisphere facing the electrode was hyperpolarized while the other side was depolarized during anodic stimulation. (C) Time course of the magnitude of Φ_m at 0° reached steady state in less than 2 μs and the membrane discharged with the same time constant after stimulation was switched off. In B and C, the electrode-to-cell distance was 2.5 times the cell radius.

distance, the degree of polarization in the hemisphere toward the electrode was increased as the electrode-to-cell distance was decreased (i.e., greater asymmetry). The location of the neutral point was also a function of electrode-to-cell distance. The neutral point at smaller electrode-to-cell distances was further from the equator than the neutral point at larger electrode-to-cell distances, both during the transient phase of membrane polarization and during the steady state [Fig. 5(B)]. The magnitude of transmembrane polarization was inversely related to the electrode-to-cell distance and decreased rapidly as the electrode-to-cell distance increased [Fig. 5(C)], but the time course of polarization was unaffected. The time course of Φ_m at two different electrode-to-cell distances (2.5R and 4R) are compared in Fig. 5(D), and the normalized trace makes clear that the time course of Φ_m was independent of the electrode-to-cell distance.

The presence of the cell altered the distribution and magnitude of the intracellular and extracellular potentials (Fig. 2), and subsequently the magnitude of Φ_m was changed. The amplitude of Φ_m over both the hyperpolarized and depolarized portions of the cell was increased [Fig. 6(A)] when the potentials were calculated with the cell present. The maximum Φ_m when the potentials were calculated without considering the presence of the cell was estimated as the potential difference between $r = 0$ and $r = R$ in Fig. 2(D), and was less than the Φ_m determined with the cell present. To quantify the degree to which the altered field increased Φ_m, the maximum polarizations (V_{cp}: with cell present and V_{ca}: with cell absent) were compared at different electrode-to-cell distances [Fig. 6(B)]. When

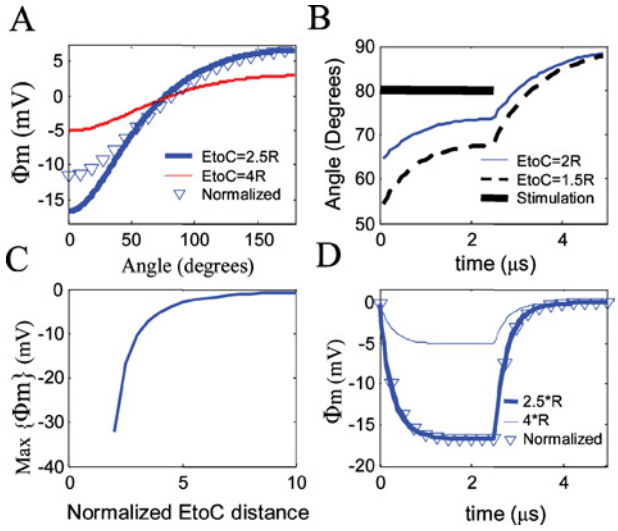

FIGURE 5. Effect of electrode-to-cell distance (EtoC) on cell polarization. (A) Transmembrane potential at two different electrode-to-cell distances with a cell radius of 10 μm. To compare the patterns of Φ_m, Φ_m at 4R was normalized. (B) Neutral point (angle where $\Phi_m = 0$) at steady state was also a function of the electrode-to-cell distance. During the application of the stimulus current, the neutral point shifted toward the equator with the same time constant as membrane polarization. (C) Magnitude of the maximum transmembrane voltage decreased as the electrode-to-cell distance increased ($R = 10$ μm). (D) The electrode-to-cell distance influence the magnitude of Φ_m, but the cellar time constant (τ_c) showed little difference.

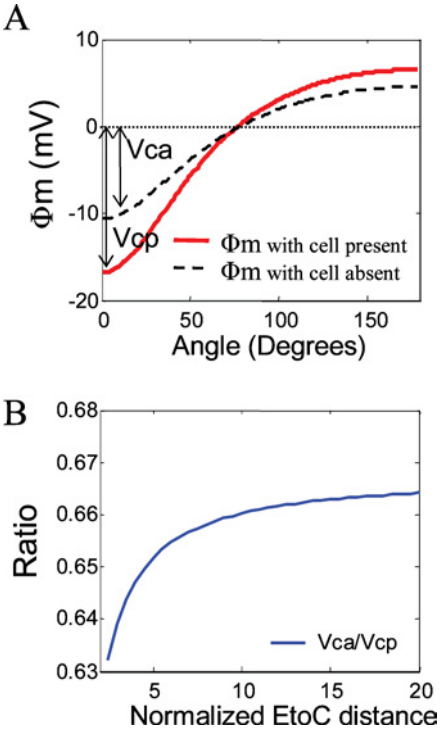

FIGURE 6. Influence of the presence of the cell on the transmembrane voltage. (A) Φ_m with the cell present was compared to the Φ_m estimated from the electric field calculated without considering the presence of the cell. Φ_m in this case was computed from the potential difference between the origin (the center point of the cell if the cell were present) and the cell radius (if the cell were present). (B) Ratio of maximum polarization amplitudes obtained with and without the cell present (V_{ca}: maximum polarization with cell absent and V_{cp}: with cell present).

the effect of the altered electric field was ignored, the magnitude of Φ_m was underestimated by 33–37%.

Comparison with Transmembrane Voltage in Uniform Extracellular Field

The Φ_m of the spherical cell in a nonuniform electric field exhibited asymmetric biphasic polarization, and the degree of asymmetry and position of the neutral point were dependent on the electrode-to-cell distance. The Φ_m in a uniform field exhibited symmetric biphasic polarization and the neutral point was always at the equator (90°). The Φ_m in a uniform field (cosine function, Eq. 10) was compared to the Φ_m in a nonuniform field as a function of the electrode-to-cell distance (Fig. 7). As the electrode was moved farther from the cell, the pattern of Φ_m generated in the nonuniform field approached the pattern of Φ_m generated in the uniform field.

To quantify the differences in polarization a percent error between the Φ_m resulting from a nonuniform field and Φ_m resulting from a uniform field was calculated as a function of the electrode-to-cell distance using Eq. (13) (Fig. 7B).

$$\%\ \text{Error} = \frac{|\Phi_m^{\text{nonuniform}} - \Phi_m^{\text{uniform}}|}{|\Phi_m^{\text{nonuniform}}|} \qquad (12)$$

To achieve less than 10% difference between the Φ_m resulting from a nonuniform field and Φ_m resulting from a uniform field, the electrode-to-cell distance must exceed 13 times the cell radius.

In the uniform field the neutral point always lay at 90°, whereas in the nonuniform field the position of the neutral point was dependent on the electrode-to-cell distance. Figure 7(C) shows that as the electrode-to-cell distance increased, the neutral point at steady state shifted toward the equator. The shift of the neutral point with distance was most pronounced when the electrode was located within 10 radii of the cell. At a normalized electrode-to-cell distance of 13, where the magnitude of Φ_m in the nonuniform field was within 10% of the magnitude of Φ_m in the uniform field, the neutral point in the nonuniform field lay at 86°, as compared to 90° in the uniform field.

Sensitivity of Transmembrane Polarization to Model Parameters

The distribution, amplitude, and time course of Φ_m were studied with different values of model parameters, including the cell radius, extracellular and intracellular conductivities, and the membrane specific resistance and capacitance.

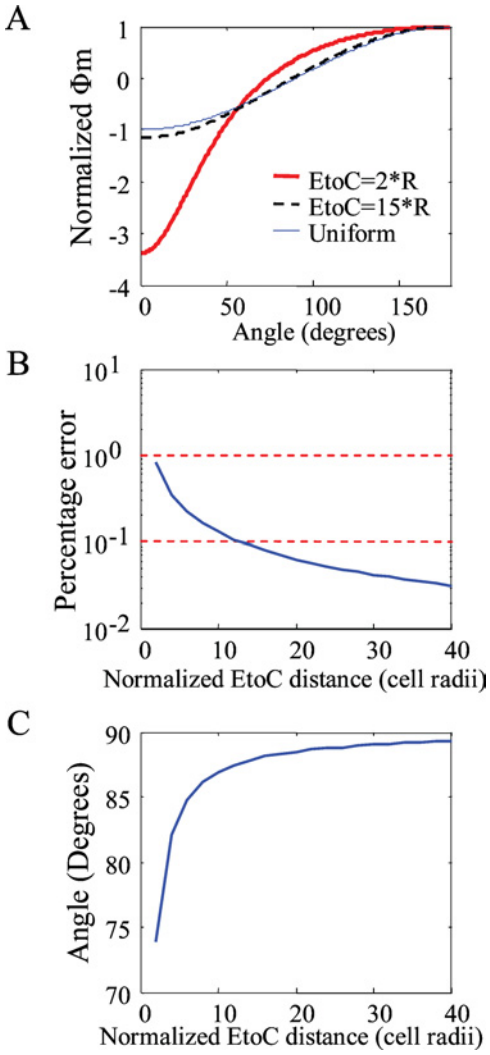

FIGURE 7. Comparison of Φ_m generated in uniform and nonuniform extracellular electric fields. (A) Patterns of Φ_m varied with different electrode-to-cell distances (EtoC). (B) Difference between transmembrane voltages generated in a nonuniform field and in a uniform field as a function of the electrode-to-cell distance. (C) Position of the neutral point (angle where ($\Phi_m = 0$) as a function of the electrode-to-cell distance, expressed in multiples of the cell radius.

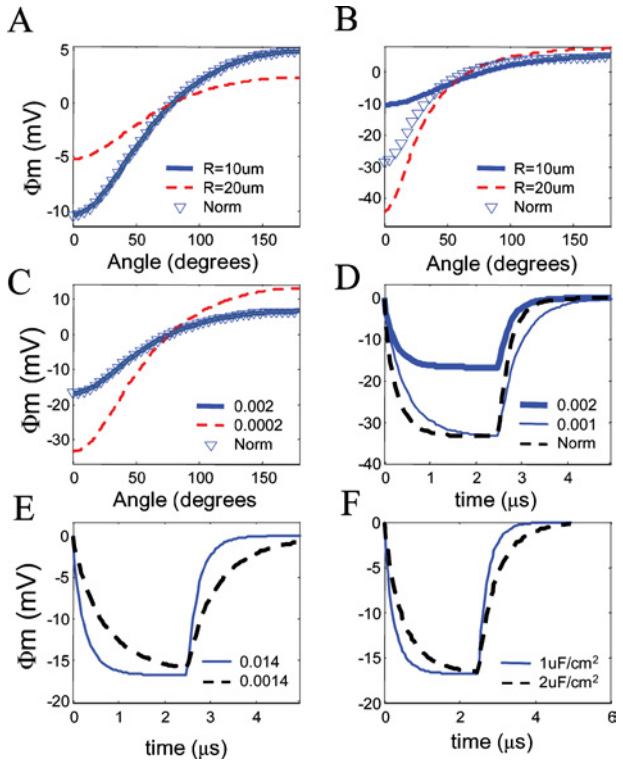

FIGURE 8. Sensitivity of transmembrane voltage to model parameters. (A) Φ_m with different cell sizes ($R = 10$ μm and 20 μm) at the same normalized electrode-to-cell distance ($X = 3$). (B) Φ_m with different cell sizes ($R = 10$ μm and 20 μm) at a fixed electrode-to-cell distance (30 μm). (C) Φ_m with different extracellular conductivities (0.002 and 0.0002 S/cm). (D) Time course of Φ_m with different extracellular conductivities (0.002 and 0.001 S/cm). (E) Time course of Φ_m with different intracellular conductivities (0.014 and 0.0014 S/cm). (F) Time course of Φ_m with different membrane specific capacitance (1 and 2 μF/cm^2).

Cell Radius

The pattern and time course of polarization were dependent on the cell radius. Figure 8(A) shows the Φ_m for two different spherical cells ($R = 10$ μm and 20 μm) at the same normalized electrode-to-cell distance ($X = 3 = d/R$, corresponding to $d = 30$ μm and 60 μm, respectively). The amplitude of Φ_m in the smaller cell was greater than the amplitude of Φ_m in the larger cell, but the patterns of Φ_m in looked similar, with both patterns exhibiting asymmetry and biphasic polarization with the neutral point located at $\sim 80^\circ$. The normalized Φ_m in Fig. 8(A) demonstrates that the patterns of Φ_m were identical at the same ratio of cell radius to electrode-to-cell distance. However, for the same two cells ($R = 10$ μm and 20 μm), located at equal physical distances from the electrode (30 μm, $X = 3$ and $X = 1.5$, respectively) the magnitude and pattern of polarization were different [Fig. 8(B)].

Conductivities of the Extracellular and Intracellular Media

Changes in the extracellular conductivity affected the magnitude, but not the pattern of Φ_m [Fig. 8(C)], while alteration of the intracellular conductivity by a factor of 10 affected neither the magnitude nor the pattern of polarization (data not shown). Reducing either the intracellular or extracellular conductivity lengthened the time constant τ_c [Figs. 8(D) and (E)], and increasing in the intracellular conductivity by a factor of 10 had approximately the same effect on τ_c as doubling the extracellular conductivity. Therefore, the τ_c of Φ_m was more sensitive to the extracellular medium conductivity than to the intracellular medium conductivity.

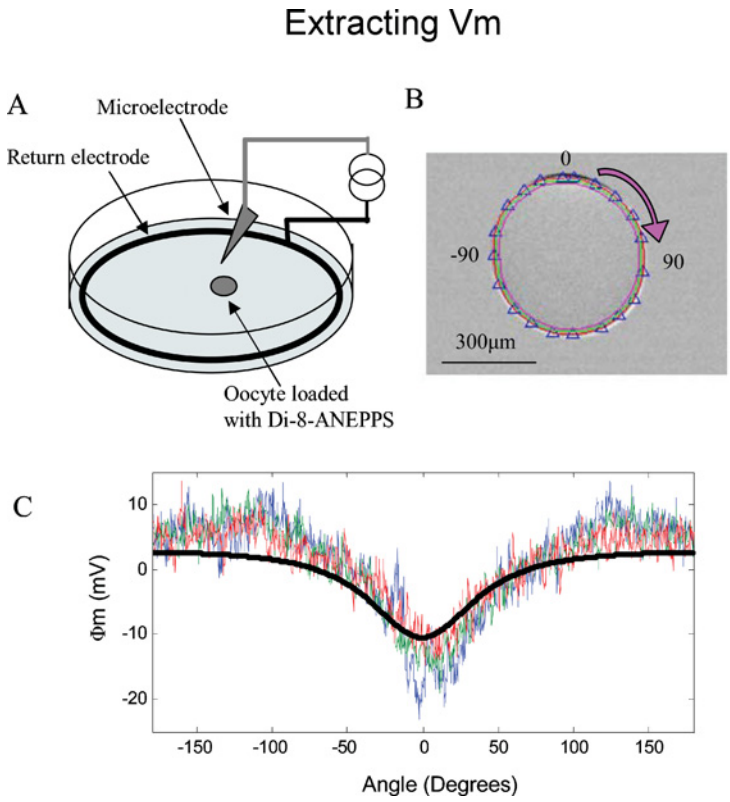

FIGURE 9. Experimental measurement of transmembrane voltage generated in a nonuniform extracellular electric field using fluorescence imaging of the voltage sensitive dye Di-8-ANEPPS. (A) A spherical cell (Xenopus oocyte) was located in the center of a Petri dish with the electrode tip located at the same height as the center of the cell. (B) Fluorescent image ($\Delta F/F$) with the line to extract Φ_m and the relative angle of the position along the oocyte with respect to the tip of the microelectrode (top view from microscope). (C) Three superimposed traces (thin lines) of the changes in fluorescence intensity with the application of the field ($\Delta F/F$), extracted from the image in B, compared to the analytical solution (thick line) for the transmembrane potential.

Specific Membrane Resistance and Capacitance

The time constant was also dependent on the membrane capacitance [Fig. 8(F)], but membrane capacitance did not affect the steady state value of Φ_m. The magnitude and pattern of polarization were insensitive to the specific membrane resistance over increases and decreases by a factor of 10.

In summary, the amplitude of Φ_m was affected by the electrode-to-cell distance, cell radius, extracellular conductivity and intracellular conductivity (data not shown), as expected from the solution (Eq. (8)). However, the normalized electrode-to-cell distance ($X = d/R$) affected only the spatial distribution of Φ_m and not its magnitude. The cellular time constant was affected by the intracellular conductivity, extracellular conductivity, cell radius, and membrane capacitance. It is clear that the membrane conductance will influence the time constant as well as the magnitude of the induced transmembrane voltage (Eqs. (10) and (11)), but for given cell and medium parameters the membrane conductance must exceed a certain limit to gain significant influence. The electrode-to-cell distance did not affect the time course of Φ_m as expected from Eq. (9).

Experimental Results

The changes in transmembrane potential generated in a nonuniform extracellular electric field were determined from fluorescence images of oocytes stained with Di-8-ANEPPS [Fig. 9(A)]. The change in intensity of the pixels along a line just inside of the cell boundary was measured, and to increase the signal-to-noise ratio, the pixel intensity values along three concentric traces were averaged [Fig. 9(B)]. The fluorescence intensity ($\Delta F/F$) was converted to voltage by assuming that a 10% change of fluorescence corresponded to a 100 mV change in Φ_m.[26] The measured Φ_m was compared with the steady state Φ_m computed from the analytical solution with model parameters selected to approximate those in the experimental setup ($\sigma_i = 0.014$ S/cm, $C_m = 4.5$ μF/cm^2, $R = 400$ μm, $\sigma_e =$ 0.002 S/cm, and stimulation intensity = 3–20 μA).[2]

The asymmetric and biphasic pattern of Φ_m determined from the analytical solution was observed in all experiments ($n = 7$ cells). With an anodic current pulse the membrane was hyperpolarized directly beneath the electrode (0°), depolarized to a lesser degree on the opposite side, and the point of zero polarization occurred at an angle of less than

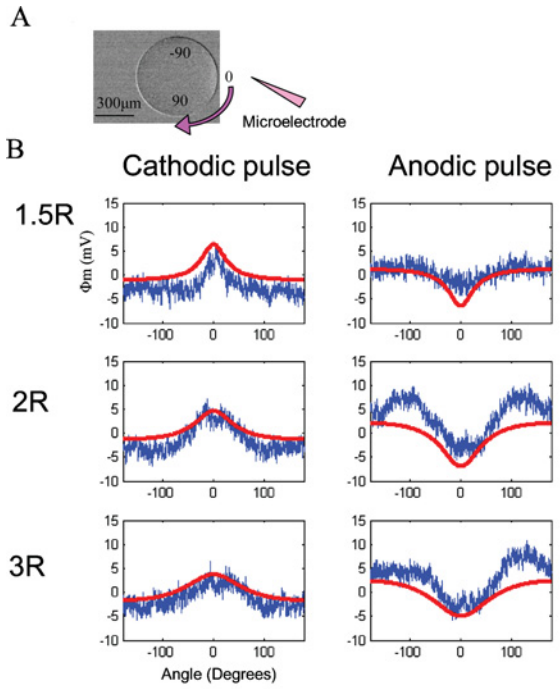

FIGURE 10. Experimental measurements of transmembrane potential generated in a spherical cell in a nonuniform electric field with different polarity (cathodic vs. anodic) current pulses and at different electrode-to-cell distances (expressed as multiples of the cell radius). (A) Fluorescent image ($\Delta F/F$) and the radial position with respect to the tip of the microelectrode. (B) The transmembrane voltages estimated from fluorescent images (thin line) and determined from the analytical solution (thick line). Each trace of experimental data is the average of three traces as described in Fig. 9. Stimulation intensities for experiment (Exp) and analytical solution (Ans) shown in B were adjusted to match the magnitude of the transmembrane potentials for cathodic stimuli (1.5R; Exp = 10 μA and Ans = 3 μA, 2R; Exp = 20 μA and Ans = 6 μA, 3R; Exp = 20 μA and Ans = 15 μA) and for anodic stimuli (1.5R; Exp = 10 μA and Ans = 3 μA, 2R; Exp = 20 μA and Ans = 9 μA, 3R; Exp = 20 μA and Ans = 20 μA).

90° [Fig. 9(C)]. The Φ_m was most asymmetric at short electrode-to-cell distances. As the electrode-to-cell distance was increased the degree of asymmetry in Φ_m was reduced and the point of zero polarization moved from more acute angles toward 90°. Finally, the sign of Φ_m was reversed by changing polarity of the stimulus (Fig. 10).

DISCUSSION

An analytical solution to Laplace's equation was derived to calculate the potentials generated in and around spherical cells by uniform and nonuniform extracellular electric fields. The distribution of potentials in the extracellular space was altered by the presence of the cell. The potential outside of top hemisphere of the cell was increased by the presence of the cell, and decreased on the opposite side. Therefore, the potentials computed ignoring the presence of the cell resulted in underestimation of the transmembrane voltage by 33–37%. This finding (33% at large electrode-to-cell distances) is equivalent to the "influential radius" factor described by Gimsa and Wachner.[11] For a spherical cell of radius R in a uniform field, the influential radius is $1.5R$, corresponding to a field amplification factor of 1.5. Thus, the maximum underestimation of transmembrane polarization without considering the change in the electric field by the presence of the cell can be computed as $(1.5R\text{-}R)/1.5R = 33\%$ in a uniform field. However, the influential radius may not be appropriate in the nonuniform field, because the electric fields are not only a function of the distance from the cell, but also the position relative to the location of the electrode tip.

Several simplifying assumptions were made to derive the analytical solution. A sphere was used to model the cell body of a neuron as this enabled derivation of an analytical solution in spherical coordinates. However, neurons may have different shapes including elliptical and stellate, and these more complex morphologies will affect the pattern of transmembrane voltage generated in the nonuniform field. Such geometries would likely require a numerical approach for determination of the distribution of transmembrane potential. Secondly, it was assumed that the extracellular medium was homogeneous. Previous experimental measurements indicate that the extracellular conductivity can vary by a factor of two in different layers of the hippocampus,[16] and this heterogeneity can influence the resulting potentials and their effect on neurons.[13] Third, the electrode was modeled as a point source of current. Previous results demonstrate that this is an adequate model at electrode-to-cell distances exceeding 10 μm, as a result of the high concentration of current density at the electrode tip.[28] However, if the electrode-to-cell distance is small, the point source assumption will result in an overestimation of the magnitude of the potentials. Further, other electrode geometries, for example bipolar pairs of electrodes or cylindrical electrodes used in clinical deep brain stimulation, will produce different distributions of extracellular potentials and generate different patterns of transmembrane potential. Fourth, the cell membrane was modeled as passive with a linear specific membrane resistance, and does not account for the dynamic activity of ion channels embedded in the membrane. Such a model provides adequate estimation of subthreshold polarization which plays an important role in initiation of subsequent nonlinear phenomena including sodium action potentials and calcium spikes. Other approaches may be employed to incorporate nonlinear membrane properties including numerical techniques,[4] and perturbational approaches,[24] but require substantially longer simulation times. Thus, while the present results do not enable predictions of the exact patterns of Φ_m in geometrically complex non-linear cells, they do provide insight into the response of such cells to a nonuniform extracellular electric field. Such information can be used to develop appropriate "cable"-type cell models, and to design electrodes

and stimulation protocols for stimulation, electroporation,[38] cell selection,[7] and cell fusion.[7,19]

In a uniform extracellular field, the top and bottom hemispheres were symmetrically but oppositely polarized, while polarization in the nonuniform field Φ_m was asymmetric with stronger polarization occurring in the portion of cell nearest to the electrode. This asymmetric biphasic polarization will result in differing effects on membrane ionic channels in different regions of the cell and will change the thresholds for excitation of cells located close to the electrode. The degree of asymmetry was reduced as the electrode was moved farther from the cell, and Φ_m in the nonuniform field approached the pattern of Φ_m generated in a uniform field. In the uniform field the neutral point was fixed at the equator (90°). In the nonuniform field the neutral point was always positioned at less than 90°, moved as a function of time, and was dependent on the electrode-to-cell distance. For cells closer to the electrode than 13 times the cell radius, the specific pattern of polarization created by the nonuniform field should be considered.

The biphasic polarization of the cell body requires special attention when modeling neurons with conventional compartmental "cable" models. Because the polarization pattern is a function of circumferential position on the cell membrane, multiple compartments are required to represent adequately the cell body. Intuitively, 6 is the minimum number of compartments required to represent the cell body,[29] and such a model exhibited the proper amplitude and pattern of polarization in a nonuniform field (data not shown).

In addition to its implications for modeling of the cell body, the alteration of the electric field caused by the presence of the cell may affect the polarization and excitation of presynaptic terminals in the vicinity of the cell body. The activating function at the end of a terminating axon is the first spatial difference of the potential along the fiber, and the effect of the cell on these potentials should be considered in central nervous system stimulation at short electrode-to-cell distances.

The Φ_m of the spherical cell reached steady state within a few microseconds for typically sized cell bodies. The cellular time constant (τ_c) was orders of magnitude smaller than the membrane time constant that determines the time course of Φ_m in response to intracellular current injection. The τ_c obtained from our analytical solution (Eq. (11)) was similar to experimental observations.[15] The τ_c was dependent on model parameters and was lengthened by increased extracellular (or intracellular) conductivity or decreased membrane capacitance. The short cellular time constant suggests that the membrane voltage can follow comparatively high frequency changes in the extracellular field and that membrane ion channels will be subject to rapid fluctuations in transmembrane voltage during alternating field stimulation.

The pattern of Φ_m calculated analytically was validated by fluorescence images of oocytes in a nonuniform field. The asymmetric pattern of Φ_m generated by the nonuniform field was observed in the experiments as was the dependence of the pattern of polarization on the electrode-to-cell distance. The voltage sensitive dye Di-8-ANEPPS was used to image the pattern of polarization along the membrane because of the linearity of its voltage-induced fluorescence and its longer chain-length improves stability within the membrane.[6,26,39] Immature oocytes were selected as the cells for imaging as they have a spherical shape and passive membrane as considered in the analytical study. While the analytical solution always exhibited asymmetric polarization, the experimental estimates of Φ_m from the fluorescent images did not always exhibit clear asymmetry and there was a constant voltage shift between the calculated and measure Φ_m (Fig. 10). These differences could be due to limitations of the voltage sensitive dye including saturation of the dynamic range of fluorescence, changes in the level of background fluorescence, and the assumption of a linear relationship between the change of fluorescence and the change in transmembrane potential, and changes in the properties of the extracellular solution in the vicinity of the cell membrane as the result of ionic flux through the membrane.

APPENDIX

The procedure to obtain the coefficients in the solutions of Laplace's Equation [Eqs. (A1) and (A3)] is determined by the properties of the model defined in the Methods section, and the following steps explain how the coefficients were computed. The solutions [Eqs. (A4) and (A5)] of Laplace's Equation are the summation of associated Legendre functions. The $P_m^0[\cos\theta]$ is the mth harmonic with symmetry in γ angles. The analytical solutions were obtained by using symbolic tools in Mathematica [Wolfram Research Inc, Champaign, IL].

$$\nabla^2\Phi_i = 0 \tag{A1}$$

$$\Phi_e = \Phi_{es} + \Phi_{applied} \tag{A2}$$

$$\nabla^2\Phi_{es} = 0, \quad \Phi_{applied} = \frac{I}{4\pi\sigma_e U} \tag{A3}$$

$$\Phi_i = \sum_{m=0}^{\infty} A_m r^m P_m^0[\cos\theta], \tag{A4}$$

$$\Phi_{es} = \sum_{m=0}^{\infty} B_m r^{-(m+1)} P_m^0[\cos\theta], \tag{A5}$$

$$\Phi_e = \frac{I}{4\pi\sigma_e U} + \sum_{m=0}^{\infty} B_m r^{-(m+1)} P_m^0[\cos\theta]$$

$$= \sum_{m=0}^{\infty} (E_m + B_m) r^{-(m+1)} P_m^0[\cos\theta] \tag{A6}$$

The applied field term (Φ_{applied}) can be represented using Legendre functions with coefficients E_{m}, where the E_{m} are functions of time and distance (U) between electrode and a specific point for potential. Due to the axial symmetry, U can be represented in spherical coordinates as a function of R (cell radius), d (distance from the origin to the electrode) and θ (radial displacement). The coefficients E_{m} in spherical coordinates are

$$E_{\text{m}} = \frac{I \times r^{1+m} P_1}{4\pi P_2}$$

$$P_1 = \int_0^{\pi} \frac{\sin\theta P_{\text{m}}[\cos\theta]}{\sqrt{R^2 + d^2 - 2Rd\,\cos\theta}}\, d\theta,$$

$$P_2 = \int_0^{\pi} \sin\theta P_{\text{m}}[\cos\theta]^2\, d\theta$$

Next, we solve the two coefficients A_{m} and B_{m} which are functions of time, because the applied current is a function of time. The associated Legendre functions are orthogonal to each other with different m. Therefore, the solution can be obtained for each m in the summation of Legendre functions. Then each coefficient (A_{m} and B_{m}) is presented as only a function of time in each m value, A and B.

Plugging the solutions, Eqs. (A4) and (A6), into the boundary conditions, Eqs. (A7) and (A8), produces first order differential equations, Eqs. (A9) and (A10), where V_{r} is the resting potential.

$$\sigma_{\text{i}} \frac{\partial \Phi_{\text{i}}}{\partial r} = C_{\text{m}} \frac{\partial \Phi_{\text{m}}}{\partial t} + \frac{\Phi_{\text{m}}}{R_{\text{m}}}, \quad \Phi_{\text{m}} = \Phi_{\text{i}} - \Phi_{\text{e}} \tag{A7}$$

$$\sigma_{\text{i}} \frac{\partial \Phi_{\text{i}}}{\partial r} = \sigma_{\text{e}} \frac{\partial \Phi_{\text{e}}}{\partial r} \tag{A8}$$

$$f_1 A + f_2 A' + g_1 B + g_2 B' + j_1 I + j_2 I' + j_3 V\text{r} = 0, \tag{A9}$$

$$h_1 A + h_2 B + m_1 I = 0, \tag{A10}$$

To solve Eq. (A9), we need one more equation which is the derivative of Eq. (A10) by time [Eq. (A11)],

$$h_1 A' + h_2 B' + m_1 I' = 0, \tag{A11}$$

The coefficients in (A9)–(A11) are defined below.

$$h_1 = R^{-1+m} m \sigma_{\text{i}} P_{\text{m}}[\cos\theta],$$

$$h_2 = R^{-2-m}(1+m)\sigma_{\text{e}} P_{\text{m}}[\cos\theta], \quad m_1 = \frac{P_{\text{m}}[\cos\theta] P_3}{4 P_2 \pi}$$

$$f_1 = \frac{R^{-1+m}(R + m\sigma_{\text{i}} R_{\text{m}}) P_{\text{m}}[\cos\theta]}{R_{\text{m}}},$$

$$f_2 = R^{\text{m}} C_{\text{m}} P_{\text{m}}[\cos\theta], \quad g_1 = -\frac{R^{-1-m} P_{\text{m}}[\cos\theta]}{R_{\text{m}}},$$

$$g_2 = -R^{-1-m} C_{\text{m}} P_{\text{m}}[\cos\theta]$$

$$j_1 = -\frac{P_1 P_{\text{m}}[\cos\theta]}{4\pi\sigma_{\text{e}} P_2 R_{\text{m}}}, \quad j_2 = -\frac{C_{\text{m}} P_1 P_{\text{m}}[\cos\theta]}{4\pi\sigma_{\text{e}} P_1},$$

$$j_3 = -\frac{1}{R_{\text{m}}}$$

$$P_3 = \int_0^{\pi} \frac{(R - d\cos\theta)\sin\theta P_{\text{m}}[\cos\theta]}{(R^2 + d^2 - 2Rd\cos\theta)^{3/2}}\, d\theta$$

Using Eqs. (A10) and (A11), Eq. (A9) can be represented as a function of only A, A', I, and I'.

$$\frac{(f_1 h_2 - g_1 h_1)}{(f_2 h_2 - g_2 h_1)} A + A' = \frac{(g_1 m_1 - h_2 j_1)}{(f_2 h_2 - g_2 h_1)} I + \frac{(g_2 m_1 - h_2 j_2)}{(f_2 h_2 - g_2 h_1)} I' - \frac{(h_2 j_3)}{(f_2 h_2 - g_2 h_1)} V r, \tag{A12}$$

and can be simplified to

$$A' + a_1 A = f_a s + a_4 V r, \tag{A13}$$

$$a_1 = \frac{(f_1 h_2 - g_1 h_1)}{(f_2 h_2 - g_2 h_1)}, \quad a_2 = \frac{(g_1 m_1 - h_2 j_1)}{(f_2 h_2 - g_2 h_1)},$$

$$a_3 = \frac{(g_2 m_1 - h_2 j_2)}{(f_2 h_2 - g_2 h_1)}, \quad a_4 = -\frac{(h_2 j_3)}{(f_2 h_2 - g_2 h_1)},$$

$$f_a s = a_2 I + a_3 I'$$

where the term s is a function of time.

The general solution of Eq. (A12) is

$$A = e^{-a_1 t} \int_0^t (C + e^{a_1 t}(a_4 V r + f_{a1} s[\tau])\, d\tau \tag{A14}$$

The constant C will be zero under the initial condition that potential equal to zero at $t = 0$. Following the same procedure, B was obtained as

$$B = e^{-b_1 t} \int_0^t e^{b_1 t}(b_4 V r + f_b s[\tau])\, d\tau \tag{A15}$$

$$b_1 = \frac{(g_1 h_1 - f_1 h_2)}{(g_2 h_1 - f_2 h_2)}, \quad b_2 = \frac{(f_1 m_1 - h_1 j_1)}{(g_2 h_1 - f_2 h_2)},$$

$$b_3 = \frac{(f_2 m_1 - h_1 j_2)}{(g_2 h_1 - f_2 h_2)}, \quad b_4 = -\frac{(h_1 j_3)}{(g_2 h_1 - f_2 h_2)},$$

$$f_b s = b_2 I + b_3 I'$$

In computing the infinite summation of Legendre functions, only the first 20 terms ($m = 20$) were used, and increasing m did not make any substantial improvement in the accuracy of the solutions.

Under the condition that the rest potential is zero ($V_{\text{r}} = 0$) and the applied current is a square pulse (unit step function) with pulse width t_1 and intensity S_{c}, the coefficients A and B are the integration of the step and delta functions.

$$A = e^{-a_1 t} \int_{00}^{t_1} (a_2 S_{\text{c}} \text{UnitStep}\,[t] + a_3 S_{\text{c}}\,\text{Delta}\,[t]) e^{a_1 t} d\tau$$

$$= \frac{a_2}{a_1} S_{\text{c}} e^{-a_1 t}(e^{a_1 t} - 1), \quad t < t_1$$

$$= \frac{a_2}{a_1} S_{\text{c}}(1 - e^{-a_1 t}), \tag{A16}$$

and

$$B = \frac{b_2}{b_1} S_c (1 - e^{-b_1 t}) \tag{A17}$$

Therefore, the steady state values of A and B are a_2/a_1 and b_2/b_1 with time constants a_1 and b_1 for the intracellular and extracellular media, respectively.

$$\frac{a_2}{a_1} = \frac{(g_1 m_1 - h_2 j_1)}{(f_1 h_2 - g_1 h_1)}$$

$$= \frac{\left(-\frac{R^{-1-m} P_m[\cos\theta]}{R_m} \frac{P_m[\cos\theta] P_3}{4 P_2 \pi} + R^{-2-m}(1+m)\sigma_e P_m[\cos\theta] \frac{P_1 P_m[\cos\theta]}{4\pi\sigma_e P_2 R_m}\right)}{\left(\frac{R^{-1+m}(R+m\sigma_i R_m) P_m[\cos\theta]}{R_m} R^{-2-m}(1+m)\sigma_e P_m[\cos\theta] + \frac{R^{-1-m} P_m[\cos\theta]}{R_m} R^{-1+m}\sigma_i m P_m[\cos\theta]\right)}$$

$$= \frac{R^{1-m}(-R \times P_3 + (1+m) P_1)}{4 P_2 \pi ((R + m\sigma_i R_m)(1+m)\sigma_e + mR\sigma_i)}$$

$$= \frac{R^{1-m}\left(-R \int_0^\pi \frac{(R - d\ \cos\theta)\ \sin\theta P_m[\cos\theta]}{(R^2 + d^2 - 2Rd\ \cos\theta)^{3/2}} d\theta + (1+m)\int_0^\pi \frac{\sin\theta P_m[\cos\theta]}{\sqrt{R^2 + d^2 - 2Rd\cos\theta}} d\theta\right)}{4\pi((R + m\sigma_i R_m)\cdot(1+m)\sigma_e + mR\sigma_i)\int_0^\pi \sin\theta P_m[\cos\theta]^2\, d\theta}$$

With the condition that the membrane is much less conductive than the intracellular and extracellular media ($1/R_m \ll \sigma_i, \sigma_e$) and $X = d/R$[22] the normalized electrode-to-cell distance, the former equation can be simplified to

$$\frac{a_2}{a_1} = \left[R^{-m}\left(-\int_0^\pi \frac{(1 - X\ \cos\theta)\ \sin\theta P_m[\cos\theta]}{(1 + X^2 - 2X\ \cos\theta)^{3/2}} d\theta + (1+m)\int_0^\pi \frac{\sin\theta P_m[\cos\theta]}{\sqrt{1 + X^2 - 2X\cos\theta}} d\theta\right)\right] \Big/ \left[4\pi\sigma_i\sigma_e R_m\left(\frac{1+m}{m}\right)\int_0^\pi \sin\theta P_m[\cos\theta]^2\, d\theta\right] \tag{A18}$$

The solution for the transmembrane voltage is the difference between the solutions for the intracellular and extracellular potentials at $r = R$. Plugging a_2/a_1 into the Eq. (A4) at $r = R$ illustrates that the potential is only a function of X (normalized electrode-to-cell distance), as shown in Fig. 4(C).

The time constants of each coefficient of the mth harmonic Legendre function are

$$a_1 = \frac{(f_1 h_2 - g_1 h_1)}{(f_2 h_2 - g_2 h_1)}$$

$$= \left[\left(\frac{R^{-1+m}(R + m\sigma_i R_m) P_m[\cos\theta]}{R_m}\right) R^{-2-m}(1+m)\sigma_e \times P_m[\cos\theta] + \frac{R^{-1-m} P_m[\cos\theta]}{R_m} R^{-1+m} m\sigma_i P_m[\cos\theta]\right] \Big/ \left[(R^m C_m P_m[\cos\theta] R^{-2-m}(1+m)\sigma_e P_m[\cos\theta] + R^{-1-m} C_m P_m[\cos\theta] R^{-1+m} m\sigma_i P_m[\cos\theta])\right]$$

$$= \frac{(R^{-1}(R + m\sigma_i R_m)(1+m)\sigma_e + m\sigma_i)}{R_m C_m((1+m)\sigma_e + m\sigma_i)}$$

$$b_1 = \frac{(g_1 h_1 - f_1 h_2)}{(g_2 h_1 - f_2 h_2)} = a_1 \tag{A19}$$

Under the same conditions for simplification, time constants a_1 are

$$a_1 = \frac{1}{R}\frac{1+m}{m}\frac{\sigma_e\sigma_i}{C_m((1+m)\sigma_e + m\sigma_i)}. \tag{A20}$$

ACKNOWLEDGMENTS

The authors thank Dr Jianmin Cui, Gayathri Krishnamoorthy, Hua Pan, and Lei Hu for supplying oocytes, Dr Dimitri Kourennyi and Xiaodong Liu for assistance in acquiring fluorescence images, and Dr Igor Efimov for review and critique. This project was supported by National Institutes of Health Grant No. R01 NS-40894.

REFERENCES

[1] Altman, K. W., and R. Plonsey. Development of a model for point source electrical fibre bundle stimulation. *Med. Biol. Eng. Comput.* 26:466–475, 1988.

[2] Baumgartner, W., L. Islas, and F. J. Sigworth. Two-microelectrode voltage clamp of Xenopus oocytes: Voltage errors and compensation for local current flow. *Biophys. J.* 77:1980–1991, 1999.

[3] Bernhardt, J., and H. Pauly. On the generation of potential differences across the membranes of ellipsoidal cells in an alternating electrical field. *Biophysik* 10:89–98, 1973.

[4] Buitenweg, J. R., W. L. Rutten, and E. Marani. Geometry-based finite-element modeling of the electrical contact between a cultured neuron and a microelectrode. *IEEE Trans. Biomed. Eng.* 50:501–509, 2003.

[5]Cartee, L. A., and R. Plonsey. The transient subthreshold response of spherical and cylindrical cell models to extracellular stimulation. *IEEE Tran.s Biomed. Eng.* 39:76–85, 1992.
[6]Ehrenberg, B., D. L. Farkas, E. N. Fluhler, Z. Lojewska, and L. M. Loew. Membrane potential induced by external electric field pulses can be followed with a potentiometric dye. *Biophys. J.* 51:833–837, 1987.
[7]Eppich, H. M., R. Foxall, K. Gaynor, D. Dombkowski, N. Miura, T. Cheng, S. Silva-Arrieta, R. H. Evans, J. A. Mangano, F. I. Preffer, and D. T. Scadden. Pulsed electric fields for selection of hematopoietic cells and depletion of tumor cell contaminants. *Nat. Biotechnol.* 18:882–887, 2000.
[8]Foster, K. R., J. M. Bidinger, and D. O. Carpenter. The electrical resistivity of cytoplasm. *Biophys. J.* 16:991–1001, 1976.
[9]Garonzik, I. M., S. E. Hua, S. Ohara, and F. A. Lenz. Intraoperative microelectrode and semi-microelectrode recording during the physiological localization of the thalamic nucleus ventral intermediate. *Mov. Disord.* 17(Suppl. 3):S135–S144, 2002.
[10]Geddes, L. A., and L. E. Baker. The specific resistance of biological material–A compendium of data for the biomedical engineer and physiologist. *Med. Biol. Eng.* 5:271–293, 1967.
[11]Gimsa, J., and D. Wachner. On the analytical description of transmembrane voltage induced on spheroidal cells with zero membrane conductance. *Eur. Biophys. J.* 30:463–466, 2001.
[12]Gimsa, J., and D. Wachner. Analytical description of the transmembrane voltage induced on arbitrarily oriented ellipsoidal and cylindrical cells. *Biophys. J.* 81:1888–1896, 2001.
[13]Grill, W. M., Jr. Modeling the effects of electric fields on nerve fibers: Influence of tissue electrical properties. *IEEE Trans. Biomed. Eng.* 46:918–928, 1999.
[14]Grill, W. M., N. Bhadra, and B. Wang. Bladder and urethral pressures evoked by microstimulation of the sacral spinal cord in cats. *Brain Res.* 836:19–30, 1999.
[15]Hibino, M., H. Itoh, and K. Kinosita, Jr. Time courses of cell electroporation as revealed by submicrosecond imaging of transmembrane potential. *Biophys. J.* 64:1789–1800, 1993.
[16]Holsheimer, J. Electrical conductivity of the hippocampal CA1 layers and application to current-source-density analysis. *Exp. Brain Res.* 67:402–410, 1987.
[17]Jerry, R. A., A. S. Popel, and W. E. Brownell. Potential distribution for a spheroidal cell having a conductive membrane in an electric field. *IEEE Trans. Biomed. Eng.* 43:970–972, 1996.
[18]Jezernik, S., M. Craggs, W. M. Grill, G. Creasey, and N. J. Rijkhoff. Electrical stimulation for the treatment of bladder dysfunction: Current status and future possibilities. *Neurol. Res.* 24:413–430, 2002.
[19]Kanamori, H., and J. N. Siegel. Induction of erythroid gene expression by microcell fusion. *Exp. Cell Res.* 232:90–96, 1997.
[20]Klee, M., and R. Plonsey. Stimulation of spheroidal cells–The role of cell shape. *IEEE Trans. Biomed. Eng.* 23:347–354, 1976.
[21]Kotnik, T., and D. Miklavcic. Analytical description of transmembrane voltage induced by electric fields on spheroidal cells. *Biophys. J.* 79:670–679, 2000.
[22]Kotnik, T., D. Miklavcic, and T. Slivnik. Time course of transmembrane voltage induced by time-varying electric field—A method for theoretical analysis and its application. *Bioelectrochem. Bioenerg.* 45:3–16, 1998.
[23]Krassowska, W. Field stimulation of cardiac fibers with random spatial structure. *IEEE Trans. Biomed. Eng.* 50:33–40, 2003.
[24]Krassowska, W., and J. C. Neu. Response of a single cell to an external electric field. *Biophys. J.* 66:1768–1776, 1994.
[25]Leon, L. J., and F. A. Roberge. A model study of extracellular stimulation of cardiac cells. *IEEE Trans. Biomed. Eng.* 40:1307–1319, 1993.
[26]Loew, L. M. Voltage-sensitive dyes: Measurement of membrane potentials induced by DC and AC electric fields. *Bioelectromagnetics* (Suppl. 1):179–189, 1992.
[27]Marszalek, P., D. S. Liu, and T. Y. Tsong. Schwan equation and transmembrane potential induced by alternating electric field. *Biophys. J.* 58:1053–1058, 1990.
[28]McIntyre, C. C., and W. M. Grill. Finite element analysis of the current-density and electric field generated by metal microelectrodes. *Ann. Biomed. Eng.* 29:227–235, 2001.
[29]McIntyre, C. C., and W. M. Grill. Extracellular stimulation of central neurons: Influence of stimulus waveform and frequency on neuronal output. *J. Neurophysiol.* 88:1592–1604, 2002.
[30]Mushahwar, V. K., D. F. Collins, and A. Prochazka. Spinal cord microstimulation generates functional limb movements in chronically implanted cats. *Exp. Neurol.* 163:422–429, 2000.
[31]Mushahwar, V. K., D. M. Gillard, M. J. Gauthier, and A. Prochazka. Intraspinal micro stimulation generates locomotor-like and feedback-controlled movements. *IEEE Trans. Neural Syst. Rehabil. Eng.* 10:68–81, 2002.
[32]Nicholson, P. W. Specific impedance of cerebral white matter. *Exp. Neurol.* 13:386–401, 1965.
[33]Plonsey, R., and R. C. Barr. Bioelectricity: A Quantitative Approach, 2nd ed. New York: Kluwer Academic, 2000.
[34]Pucihar, G., T. Kotnik, M. Kanduser, and D. Miklavcic. The influence of medium conductivity on electropermeabilization and survival of cells in vitro. *Bioelectrochemistry* 54:107–115, 2001.
[35]Rall, W., I. Segev, J. Rinzel, and G. M. Shepherd. The Theoretical Foundation of Dendritic Function: Selected Papers of Wilfrid Rall with Commentaries. Cambridge, MA.: MIT Press, 1995.
[36]Roth, B. J., and W. Krassowska. The induction of reentry in cardiac tissue. The missing link: How electric fields alter transmembrane potential. *Chaos* 8:204–220, 1998.
[37]Schwan, H. P. Electrical properties of tissue and cell suspensions. *Adv. Biol. Med. Phys.* 5:147–209, 1957.
[38]Weaver, J. C. Electroporation theory. Concepts and mechanisms. *Methods Mol. Biol.* 47:1–26, 1995.
[39]Wu, J. Y., C. X. Falk, L. Cohen, Y. Tsau, and D. Zecevic. Optical measurement of action potential activity in invertebrate ganglia. *Jpn. J. Physiol.* 43(Suppl. 1):S21–S29, 1993.
[40]Zhang, J., R. M. Davidson, M. D. Wei, and L. M. Loew. Membrane electric properties by combined patch clamp and fluorescence ratio imaging in single neurons. *Biophys. J.* 74:48–53, 1998.